NEUROSCIENCE

Dynamic coding of predatory information between the prelimbic cortex and lateral amygdala in foraging rats

Eun Joo Kim,[1] Mi-Seon Kong,[1] Sang Geon Park,[2] Sheri J. Y. Mizumori,[1,3] Jeiwon Cho,[4,5,6]* Jeansok J. Kim[1,3]*

Predation is considered a major selective pressure in the evolution of fear, but the neurophysiology of predator-induced fear is unknown. We simultaneously recorded lateral amygdala (LA) and prelimbic (PL) area neuronal activities as rats exited a safe nest to search for food in an open space before, during, and after encountering a "predator" robot programmed to surge from afar. Distinct populations of LA neurons transiently increased spiking as rats either advanced or fled the robot, whereas PL neurons showed longer-lasting spike trains that preceded and persisted beyond LA activity. Moreover, discrete LA-PL cell pairs displayed correlated firings only when the animals either approached or fled the robot. These results suggest a general fear function of the LA-PL circuit where the PL participates in the initial detection of potential threats, the LA signals the occurrence of real threats, and the dynamic LA-PL interaction optimizes defensive readiness for action.

INTRODUCTION

Fear is an integral part of the brain's defensive mechanism that evolved to guide and shape behaviors of animals and humans against predation and other ecological risks (*1*–*3*). However, contemporary models of fear largely developed from rodent Pavlovian fear conditioning research that basically focuses on how a particular conditioned stimulus (CS; such as tone, light, and context), upon contingent pairing with a noxious unconditioned stimulus (US; usually footshock) that automatically elicits defensive unconditioned responses (mostly pain reflex), becomes capable of emitting discrete conditioned fear responses (CRs; typically freezing) autonomously (*4*–*8*). It is now well accepted that the amygdala plays a central role in both learned and innate fear behaviors (*9*–*12*). Recent studies have further suggested that the amygdala and the medial prefrontal cortex (mPFC) critically interact during fear conditioning (*4*, *13*–*15*). Specifically, the basolateral (BL) complex of the amygdala (BLA), composed of basal, accessory basal, and lateral (LA) nuclei of the amygdala (*16*), is necessary for both acquisition and expression of conditioned freezing (*17*), whereas the prelimbic (PL) cortex of the mPFC, which is monosynaptically connected with the amygdala (*18*, *19*), is critical only for the expression (and not for the acquisition) of conditioned freezing in rats (*20*). Single-unit recordings have also revealed that, following auditory fear conditioning, the tone CS–evoked neural activity in LA lasted only a fraction of a second (<100 ms), whereas the PL neural activity was elevated for the tone duration (for example, 30 s), suggesting that the transient LA response triggered tonic PL activity to sustain the behavioral expression of the CR (*13*). Highlighting the selective and cooperative functions of the BLA and PL in fear behavior, a very recent study demonstrated that the correlated firing in the BLA-PL pathway is predominantly related to a shock-associated CS than a reward-associated CS in a modified Pavlovian cue discrimination task (*21*).

Before we can make firm conclusions regarding the BLA's and PL's functions in fear, one must test BLA and PL interactions in real-world threat scenarios that require greater adaptive actions and decisions than those allowed in small experimental chambers (*2*), because it remains unknown how the characterized conditioned fear–evoked neural activities in BLA and PL operate in risky situations in nature. To address this, we used a seminaturalistic "approach food–avoid predator" paradigm (*22*, *23*) and simultaneous single-unit recordings in the BLA (specifically, LA) and PL to investigate how these neurons code and interact to process a predatory threat information in foraging rats (Fig. 1). In this behavioral task, hunger-motivated rats leaving the safety of their nest in search of food in open areas are challenged with a rapidly advancing robotic predator, which causes the animals to escape to the nest and modify their ensuing foraging behaviors. We present evidence that LA and PL dynamically alter and coordinate their neuronal activities in anticipation of and in reaction to predatory attacks.

RESULTS

The predatory robot effects on foraging time

Food-deprived rats (85% normal body weight), implanted with tetrode arrays in the LA and PL ipsilaterally, underwent successive habituation, foraging baseline, and robot test days. During the baseline sessions (5 to 10 trials per session), animals were permitted to leave the nest to search for a food pellet placed at variable locations in the foraging arena. At the start, rats cautiously explored the novel foraging arena before finding a sizeable 0.5-g pellet, which they carried back to the nest for feeding. Subsequently, rats proceeded directly to the pellet, rarely exceeding the pellet location. Tetrodes were gradually lowered until stable single units were isolated in their target structures (Fig. 1A), at which time animals underwent the robot testing, consisting of sequential "pre-robot," "robot," and "post-robot" recording phases (5 to 10 trials per phase; Fig. 1B). The mean time animals were in the foraging area (that is, time from nest exiting until either returning with the pellet or fleeing from the robot) significantly increased from 4.39 ± 0.16 s (mean ± SEM) during the pre-robot recording phase to 9.93 ± 0.51 s during the robot recording phase ($F_{2,\ 272}$ = 105.517, P < 0.001; Fig. 1, C and D) because of the animals' hesitancy to approach the pellet in the presence of the robot. Once the robot was removed, the post-robot foraging time significantly decreased to 5.40 ± 0.24 s (P < 0.001 compared to the robot), indicating decreased

[1]Department of Psychology, University of Washington, Seattle, WA 98195–1525, USA. [2]Neuroscience Program, Korea University of Science and Technology, Daejeon 34141, Republic of Korea. [3]Program in Neuroscience, University of Washington, Seattle, WA 98195–1525, USA. [4]Department of Medical Science, College of Medicine, Catholic Kwandong University, Gangneung, Gangwon-do 25601, Republic of Korea. [5]Biomedical Research Institute, International St. Mary's Hospital, Catholic Kwandong University, Incheon 22711, Republic of Korea. [6]Institute for Bio-Medical Convergence, Incheon St. Mary's Hospital, Catholic University of Korea, Incheon 22711, Republic of Korea.
*Corresponding author. Email: jeansokk@u.washington.edu (J.J.K.); jelectro21@gmail.com (J.C.)

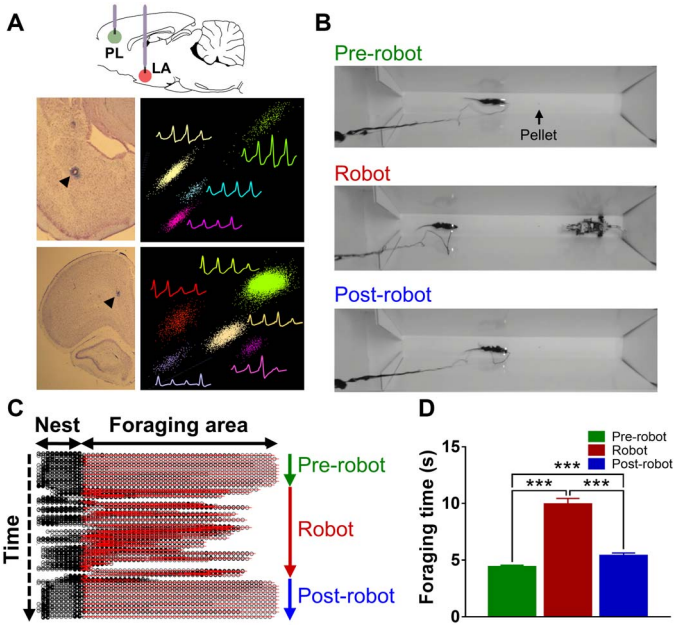

Fig. 1. Experimental design, single-unit recordings, and risky foraging behaviors. (**A**) Tetrodes were implanted targeting LA and PL simultaneously. Photomicrographs of tetrode tracks (arrowheads) and representative multiple single units recorded in the LA (upper) and PL (bottom). (**B**) Animals underwent sequential pre-robot, robot, and post-robot recording phases. During the pre- and post-robot trials, rats promptly procured the pellet. During the robot trials, every time the animals came near the pellet, the programmed robot surged toward them. (**C**) An animal's trajectory in the nest area (black) and foraging area (red) during each phase. Each line corresponds to single trials. (**D**) The foraging time increased during the robot phase compared to other phases (***$P < 0.001$ compared to the pre- and post-robot phases).

fear. However, there was a residual fear because the post-robot foraging time did not fully return to the pre-robot level ($P < 0.001$).

Classifications of LA and PL cells

A total of six rats were used, from which LA and PL neurons were simultaneously (three rats) or individually (three rats) recorded, yielding a total of 346 LA and 434 PL units (fig. S1). While rats were foraging, both LA and PL were found to show distinct categories of neural responses to either the robot (robot cells: LA, $n = 31$, 9.4%; PL, $n = 52$, 11.9%) or the food pellets (food cells: LA, $n = 15$, 4.5%; PL, $n = 43$, 9.9%; Fig. 2, A and B). There were also LA and PL cells that responded to both the robot and food pellets (both cells: LA, $n = 12$, 3.6%; PL, $n = 41$, 9.4%; fig. S2, A and B) or to neither (nonresponsive cells: LA, $n = 288$, 87.8%; PL, $n = 298$, 68.6%).

LA and PL neuronal responses to a robotic predator

The proportion of the robot-responsive LA and PL cells in the current study was comparable with previous reports, showing that a small percentage of the amygdala and PL neurons are actively involved in fear processing: LA, 4 to 12% (*24*, *25*); PL, 4 to 23% (*13*, *26*). Among the robot-responsive cells, about 48% of LA ($n = 15$) and 38% of PL ($n = 20$) cells showed their peak firing as the animals approached the stationary robot [robot-approach (RA) cells; Fig. 3, A and B]. To further explore how these neurons changed their activity, the RA cell firing rates were binned into 0.1-s epochs during the approach time zone (ATZ; see Materials and Methods) and tested with a Pearson's correlation analysis (Fig. 3C and fig. S3A). The time from robot activation was significantly correlated with the averaged LA-RA cell activity ($r = 0.863$, $P < 0.001$), but not with the PL-RA paired-cell activity ($r = 0.175$, $P = 0.534$). Although the distribution of the correlation coefficients between time and firing rates during ATZ was not different between LA-RA and PL-RA cells ($\chi^2 = 0.345$, $P = 0.557$; fig. S3B), significantly more LA-RA cells

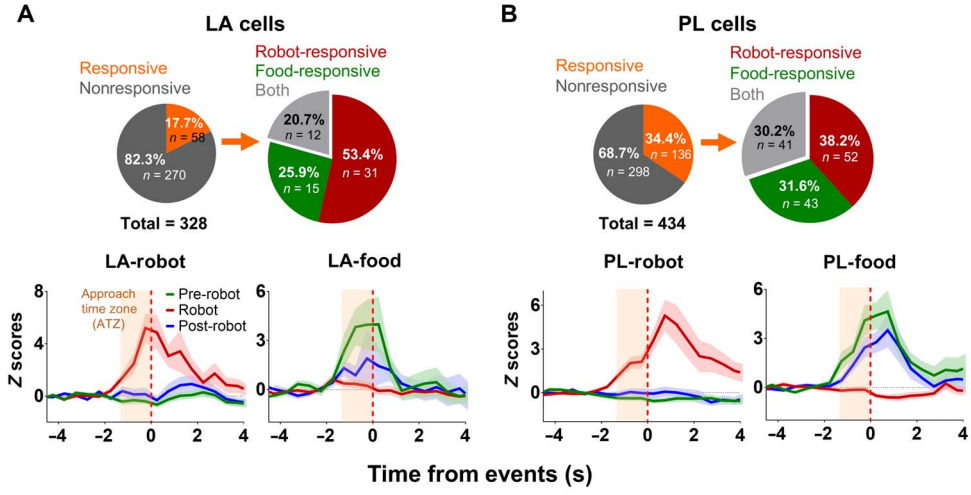

Fig. 2. Robot-responsive LA and PL units. Subsets of both LA [17.7% (**A**)] and PL [34.4% (**B**)] neurons increased firing rates to the robot, food pellet, or both. Among them, 53.4% of LA and 38.2% of PL neurons responded exclusively to the robot. ATZ (peach-shaded area) was defined as the three 0.5-s bins before the robot activation or the time when the rat reached the pellet. If the *z* score > 3 in one or more bins during the robot phase and $z < 3$ during the pre-robot phase, then the units were classified as "robot cells." The opposite criteria ($z > 3$ during the pre-robot phase; $z < 3$ during the robot phase) were used to classify "food cells." The red vertical dash line indicates the time at which the animals reached the pellet (pre- and post-robot phases) or the time at which the robot was activated (robot phase). Shaded areas indicate SEM.

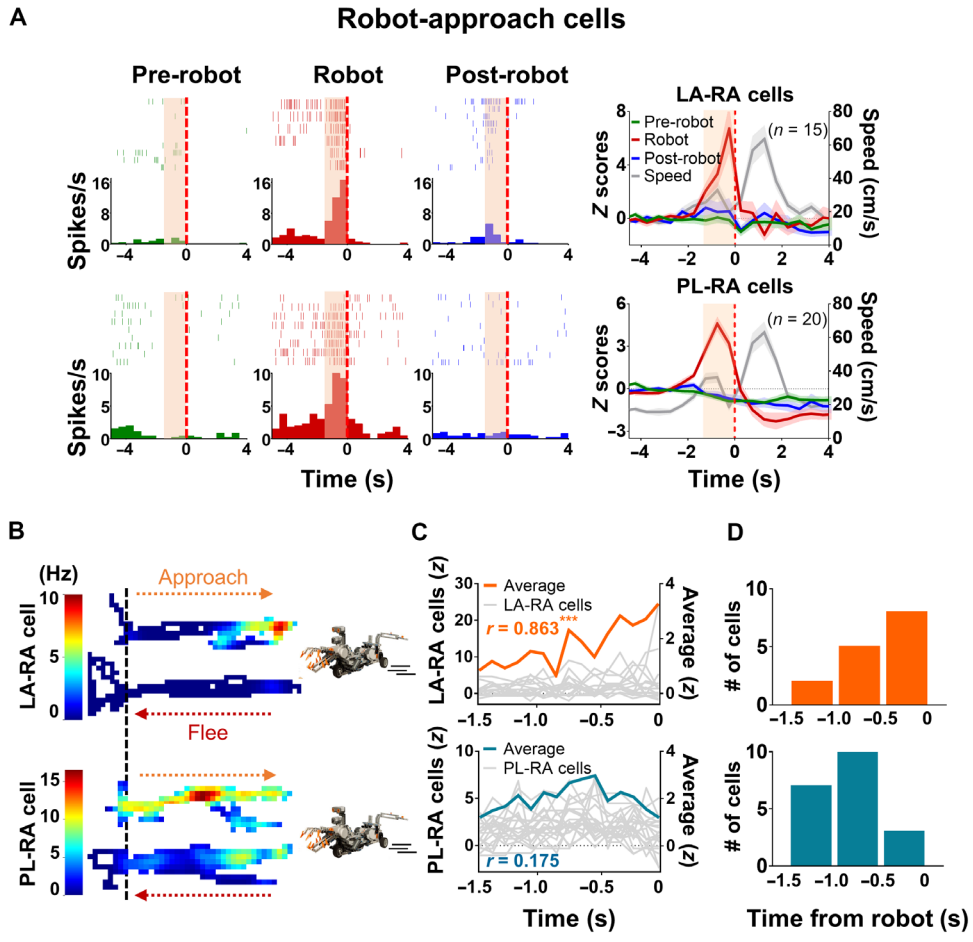

Fig. 3. RA cells in LA and PL. (**A**) A portion of classified robot cells that exhibited their maximal firing before the robot was activated (RA cells) in both LA (top) and PL (bottom). The first three columns show the representative LA-RA and PL-RA cell rasters and event histograms in each phase. The last column shows population activity of the RA cells from LA and PL and movement speeds of rats (shown in gray) around the robot activation time ($t = 0$). Peach-shaded area indicates ATZ. (**B**) Examples of firing rate maps of LA-RA and PL-RA cells during the pre-surge (−4 to 0 s before the robot activation; approach) and post-surge (0 to 4 s subsequent to robot activation; flee) epochs. The color scale for the firing rate corresponds to the firing rate (red, highest; blue, no spike) for the unit. Dashed vertical lines demarcate the nest–foraging area boundary. (**C**) During ATZ, averaged LA-RA activity linearly increased toward robot activation timing, whereas PL did not. The gray lines indicate individual LA and RA cell activities during ATZ. (**D**) The LA-RA cells tended to maximize their firing during ATZ as the rat was closer to the location of the robot, whereas the PL-RA cells increased their firing earlier than LA-RA cells (χ^2 test, $P < 0.05$). Shaded areas indicate SEM. ***$P < 0.001$.

showed their maximal responses nearer to the time of robot activation than PL-RA cells ($\chi^2 = 6.128$, $P < 0.05$; Fig. 3D). There was also a trend of the peak response latency of PL-RA cells emerging before that of LA-RA cells ($t_{33} = 1.922$, $P = 0.063$; fig. S3C). These results indicate that the RA cells in LA maximized their firing rates when rats were closer to the robotic threat and that the PL cells increased their firing earlier than the LA cells.

The remaining robot cells exhibited their maximal firing subsequent to the robot activation [robot-triggered (RT) cells; Fig. 4, A and B, and fig. S3D]. Specifically, the averaged LA-RT activity (0.1-s bin) was negatively correlated with the 1-s period after robot activation ($r = -0.773$, $P < 0.01$), whereas the PL-RT activity was positively correlated ($r = 0.965$, $P < 0.001$; Fig. 4C). The proportions of the LA-RT neurons displaying negative versus positive correlations were different from those of the PL-RT neurons ($\chi^2 = 10.685$, $P < 0.01$; fig. S3E). These results indicate that a greater number of the LA-RT neurons initially increased and then subsequently decreased their firing following the robot attack, whereas a higher percentage of the PL-RT neurons gradually increased their activity as a function of time. During the robot surge period, more LA-RT cells showed higher firing during the initial 0.5-s epoch, whereas PL-RT cells displayed higher firing during the second epoch ($\chi^2 = 4.372$, $P < 0.05$; Fig. 4D). The maximal response latency of the LA-RT cells was also shorter than that of PL-RT cells ($t_{46} = 2.147$, $P < 0.05$; fig. S3F). When RT activity was binned at 1 s to compare LA-RT with PL-RT during an extended time period (for at least 4 s), LA-RT cells showed significant increased firing (time × phase, $F_{6,\ 90} = 11.238$, $P < 0.001$) for the initial 2 s ($P < 0.05$, Bonferroni test), whereas PL-RT cells sustained their increased level of firing (time × phase, $F_{6,\ 186} = 15.126$, $P < 0.05$) at least for 4 s after robot activation ($P < 0.05$, Bonferroni test; fig. S3D). These results indicate that LA neurons immediately and briefly responded to the threat, whereas PL neurons showed delayed but persistent activity under a threat situation.

LA and PL neuronal responses to food

The food approach (FA) cells in both LA and PL decreased their firing during the robot phase despite animals advancing (albeit cautiously)

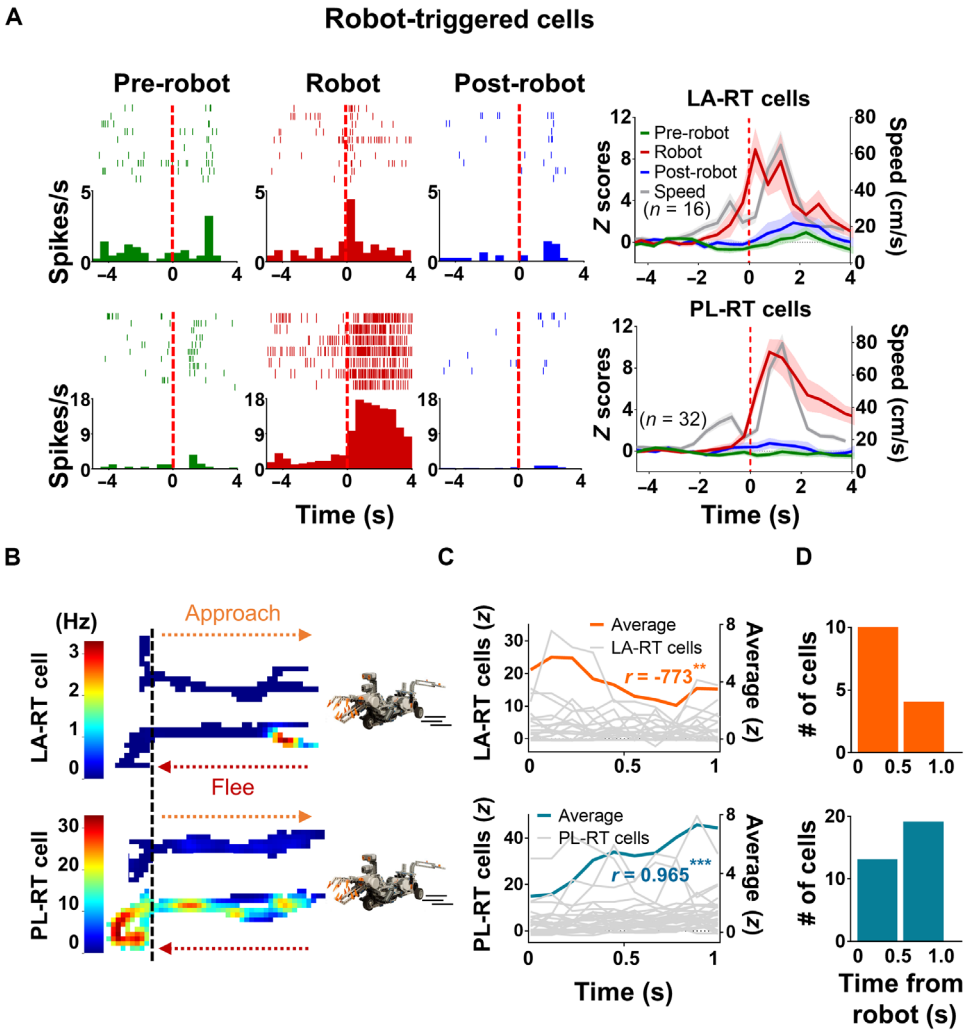

Fig. 4. RT cells in LA and PL. (**A**) Categorized robot cells that exhibited their maximal firing after the robot was activated (RT cells) in both LA (top) and PL (bottom). The first three columns show the representative LA-RT and PL-RT cells in each phase. The last column shows the population activity of RT cells in LA and PL and the movement speeds of rats (shown in gray) around the robot activation time (t = 0). (**B**) Examples of firing rate maps of LA-RT and PL-RT cells during the pre-surge (−4 to 0 s before the robot activation; approach) and surge (0 to 4 s subsequent to robot activation; flee) epochs. The color scale for the firing rate corresponds to the firing rate (red, highest; blue, no spike) for the unit. Dashed vertical lines demarcate the nest–foraging area boundary. (**C**) During the robot surge period (1 s), averaged LA-RT and PL-RT activity (0.1-s bin) linearly decreased and increased subsequent to robot activation, respectively. (**D**) During the robot surge period, LA-RT cells showed maximal firing during the initial 0.5-s bin, whereas PL-RT cells showed maximal firing during the second bin (χ^2 test, $P < 0.01$).

toward the pellet (LA: $\chi^2 = 12.250$, $P < 0.01$, Friedman test; $Z = -2.521$, $P < 0.05$, Wilcoxon test; PL: $F_{2,\ 40} = 23.691$, $P < 0.001$; fig. S4, A and B). Neither LA-FA nor PL-FA cell activities during the post-robot phase returned to their pre-robot levels ($P < 0.05$, Bonferroni test), although PL-FA cell activity significantly increased spikes compared to the robot phase ($P < 0.01$, Bonferroni test; fig. S4B). Because animals mostly were unable to procure the pellets during the robot phase (pellet success, <3%), food-responsive cells in both LA and PL did not exhibit food-triggered (FT) responses ($P < 0.05$; fig. S4C), whereas the FT responses returned to the pre-robot phase level during the post-robot phase ($P > 0.122$; fig. S4D). FA cells in LA and PL suppressed their responses while animals were facing a predatory threat, and this suppression carried over to the post-robot phase. The suppression is unlikely due to a low appetite because FT cell activities returned to the baseline level once the rat obtained the food pellet.

Neural activities and movement speed independence

We examined whether the animal's movement speed contributed to the activity changes observed for RA and RT cells. The movement speed was computed from the time animals left the nest to the time they approached the food pellet or robot (outward speed; fig. S5A). Although the outward speed decreased as the rat neared the robot compared to when the rat reached the pellet, the correlation distribution was not different between LA-RA and PL-RA cells. There was no reliable difference in the inbound speed to the nest when the animals either ran back after securing the pellet (motivated to consume; pre-robot phase) or fled from the robot (motivated to escape; robot phase). However, more RT cells in LA and PL showed significant correlation values during the robot phase than the pre-robot phase (LA: $\chi^2 = 5.236$, $P < 0.05$; PL: $\chi^2 = 15.947$, $P < 0.001$; fig. S5B). These results indicate that the robot-induced activity changes in LA and PL cannot be accounted for by the movement speed of the animals.

LA-PL cell pairs and heterogeneous responses to predatory threat

From simultaneously recorded LA (n = 216) and PL (n = 215) cells, 1099 combinatorial pairs were generated for cross-correlograms (CCs) of the pre-robot surge (4-s periods before robot activation) and post-robot surge (4-s periods subsequent to robot activation) epochs with PL cells as references. Similar CCs were examined for the pre-pellet (4-s periods before pellet procurement) and post-pellet (4-s periods subsequent to pellet procurement) epochs of the baseline phase. All recorded cells from LA and PL were included in this analysis (fig. S6). Valid cell pairs showing firing rates >0.1 Hz (both LA and PL) during the task epochs (pre-surge, 323 pairs; post-surge, 319 pairs) were further analyzed. Twenty-two CCs (from 17 LA and 20 PL cells) and 29 CCs (from 24 LA and 26 PL cells) displayed significant peaks (z scores > 3) around PL spikes (between −100 to 100 ms) during the pre-surge epoch and post-surge epoch, respectively. A repeated-measures (RM) analysis of variance (ANOVA) revealed that cell pairs that exhibited LA-PL spike synchrony during the pre-surge epoch discontinued their synchronous activity during the post-robot surge phase and when rats approached the pellet during the baseline phase (RM ANOVA, $F_{2, 42}$ = 26.484, P < 0.0001; P < 0.0001, Bonferroni test; Fig. 5A, top). In contrast, the cell pairs that showed LA-PL spike synchrony during the post-surge epoch did not show correlated firing during the pre-surge (robot phase) or post-pellet (baseline phase) epochs (RM ANOVA, $F_{2, 56}$ = 18.131, P < 0.0001; P < 0.01, Bonferroni test; Fig. 5A, bottom). On the basis of the peak position of each CC, the directionality of the LA-PL projections was inferred and analyzed. The proportion of the LA-leading (10 pairs, 45%) and PL-leading CCs (12 pairs, 55%) that

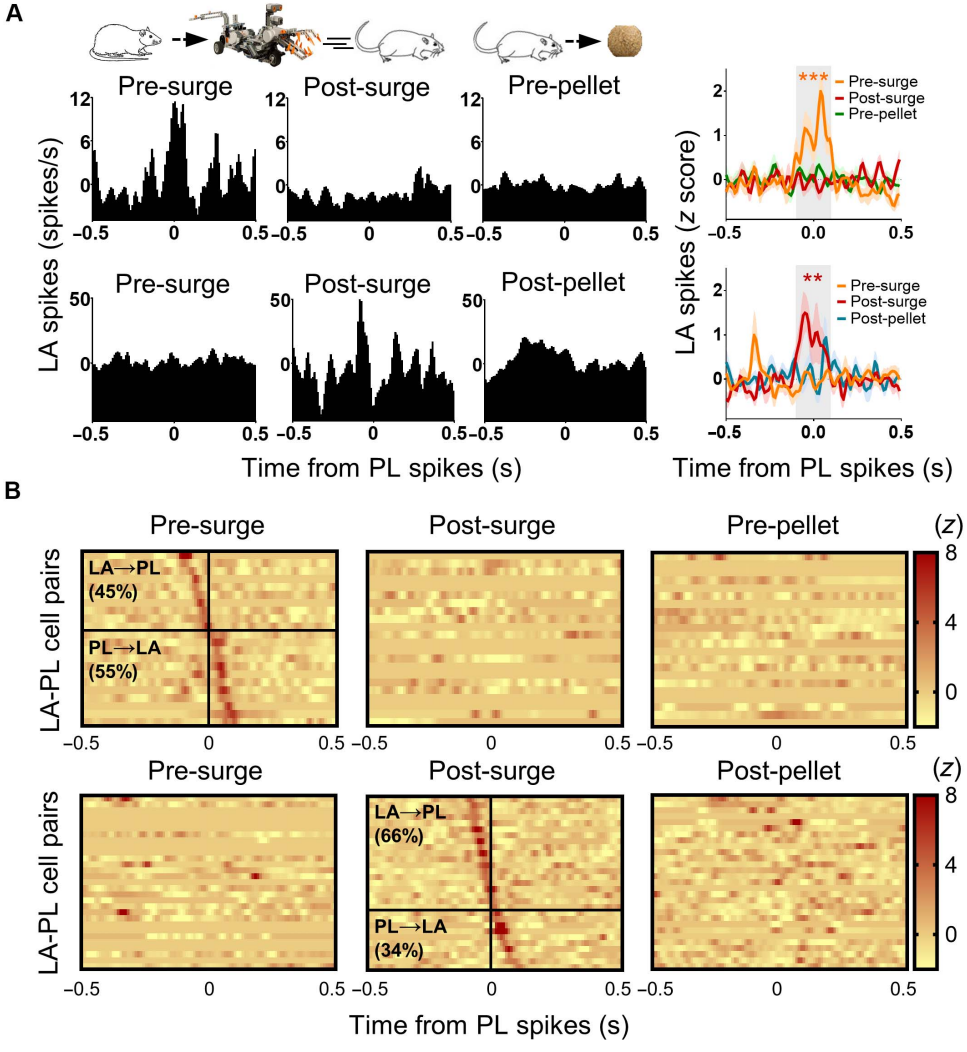

Fig. 5. Robot effects on spike synchrony between LA and PL neurons. CCs of the 1099 simultaneously recorded LA and PL cell pairs were generated for each phase with PL cells as references. (**A**) The left three columns show representative CCs of two LA-PL pairs, displaying significant spike synchrony during the 4-s epochs before (pre-surge, top) and after (post-surge, bottom) robot activation. Significant LA-PL pairs during the pre-surge and post-surge epochs were further analyzed for the 4-s epochs before (pre-pellet) and after (post-pellet) pellet procurement, respectively. The rightmost column illustrates averaged LA-PL CCs that showed significant peaks (between −100 and 100 ms; gray area) during the pre-surge (upper) or post-surge (bottom) epochs. Shaded areas indicate SEM. **P < 0.01 and ***P < 0.001, compared to the other epochs. (**B**) Color-coded CCs of all significant cell pairs that exhibited increased LA-PL spike synchrony during the pre-surge (upper) and post-surge (bottom) epochs. The vertical lines indicate the time when the reference PL spikes occurred. The horizontal lines indicate the borders between the presumable LA→PL (above the line) and PL→LA (below the line).

showed significant correlation during the pre-surge epoch were equivalent ($\chi^2 = 0.182$, $P = 0.670$; Fig. 5B). However, there was a trend for the significant LA-leading CCs (19 pairs, 66%) to be greater than the PL-leading CCs (10 pairs, 34%) during the post-surge epoch ($\chi^2 = 2.793$, $P = 0.095$; Fig. 5B).

DISCUSSION

The current understanding of the neurophysiology of fear in the LA and PL is based largely on the Pavlovian fear conditioning paradigm (*3*–*5*). Although the findings that the LA neural activity briefly increased to the CS onset (*27*, *28*) and that the PL neural activity remained elevated for the duration of the CS (*13*) may account for the expression of conditioned freezing response to a tone CS in a small chamber, it remains unknown how these differences in spiking profile after a discrete CS translate to naturalistic threat situations where animals make real-world and dynamic choices.

By using an ecologically relevant approach food-avoid predator paradigm (*22*, *23*) along with simultaneous LA and PL recordings, we found that a subset of LA neurons transiently increased spiking rates as rats either cautiously moved toward the food pellet (with a stationary robot predator on the other side of the pellet) or promptly fled the looming robot. In contrast, a subset of PL neurons showed longer-lasting spike trains that both preceded and persisted past the LA neural activity. The transient increase in the LA activity to the looming robot was considerably longer (~2 s) than what has been reported with tone CS (~100 ms); this difference cannot be accounted for by foraging rats' motion because the running speed did not correlate with the firing rates during the pre-robot and post-robot phases. Moreover, the present study revealed that PL activity could precede LA activity, PL cells show robot-evoked responses, and PL activity is uncorrelated with freezing. Unlike the LA→PL serial, static activity pattern described from fear conditioning studies (*13*, *27*), we found dynamic, bidirectional activity patterns between the LA and PL. It appears then that the nature of the neural activity is significantly different under fear conditioning situations that focus on learned fear behavior (CR) to a discrete CS versus naturalistic fear settings where the emphasis is on antipredatory responses. This view is also supported by findings that the same stimulation of the amygdala and dorsal periaqueductal gray produced completely different fear behaviors in a typical fear conditioning chamber and the present foraging arena (*29*).

A recent study recorded neural activity in the BL nucleus of the amygdala under a similar approach food-avoid predator task and reported that BL neurons increased or decreased their firing rates when rats began foraging irrespective of the presence or absence of predatory threat or reward (*30*). Thus, it was concluded that the BL activity is closely associated with the animal's movement-driving functions rather than threat signals and correlated with fear behavior, as shown here. However, there are three notable differences between the studies: (i) LA (present study) versus relatively ventral BL (*30*) recording sites; (ii) the peri-event time histogram was generated by aligning the neural activity to the robot activation (the present study) versus aligning to the animal's responses (*31*); and (iii) the fear-overcoming success rate of procuring food was extremely low (<3% in the present study; fixed pellet location and variable robot surge distances) versus considerably high (30 to 82%; variable pellet locations and fixed robot surge distance; the unit analysis included numerous pellet obtaining trials) (*30*). Regardless of these differences, the present finding of LA neurons responding to a predatory threat is consistent with previous studies that demonstrated that amygdalar lesions/inactivation selectively abolished the predatory fear (while leaving the movements associated with foraging intact) (*9*, *22*) and that localized amygdala stimulations produced fear responses in animals (*29*, *31*, *32*) and fearful reports in epileptic patients (*33*).

To account for the present results, we propose a novel neurophysiological LA-PL fear circuit model (Fig. 6) where LA and PL bidirectionally interact to weigh forthcoming and immediate threat information, and the temporal differences in the LA and PL neural activities determine the animal's defensive readiness to the predatory threats. Conceptually, this model parallels Fanselow and Lester's (*3*) theory of predatory imminence continuum, in which the topography of defensive behavior in animals is biologically determined with a particular stage in the prey-predator sequence (for example, distal versus fast-approaching predators). Specifically, the relatively early maximal activity of PL as animals progressed toward the pellet (when the robot was stationary) suggests a threat-anticipatory function of PL, whereas the maximal activity of LA that ramped up as animals moved closer to the pellet (just before the robot activation) represents the imminence of the threat (that is, the LA activity follows the PL activity). Symmetrical PL→LA and LA→PL spike synchrony also occurred while animals advanced toward a potential/imminent danger. Also, as the predator surged, the heightened LA neural activity enabled an instant escape behavior, and as animals were fleeing, the PL neurons engaged and maintained threat information processing for an extended period of time (that is, the LA activity precedes the PL activity). The elevated PL activity was observed while rats were both escaping from the looming robot and safely inside the nest and thus did not necessarily correlate with a particular fear response (such as freezing). During this time, distinct LA-PL pairs showed a tendency of asymmetrical LA→PL spike synchrony.

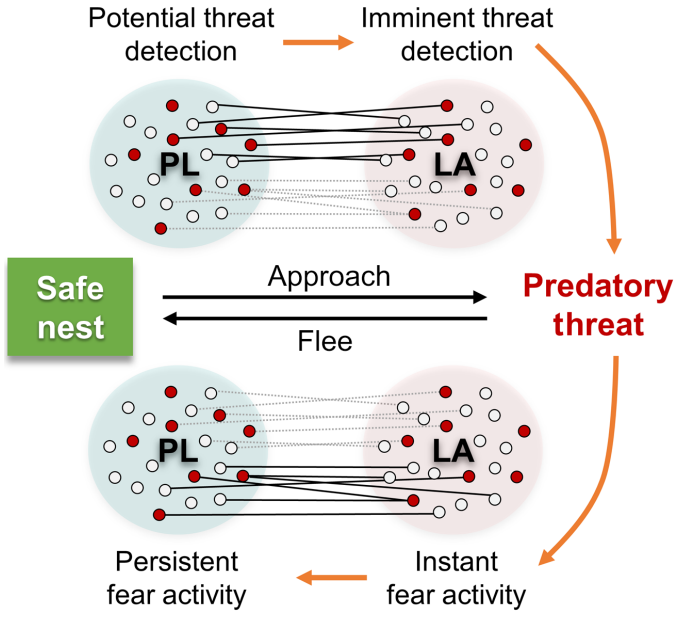

Fig. 6. A hypothesized model of LA-PL fear signaling during risky foraging in rats. LA and PL dynamically interact while rats encounter a predator during foraging. Solid and dotted lines indicate LA-PL interactions that show correlated activity and noncorrelated activity, respectively. Subsets of LA-PL pairs increased spike synchrony distinctively when the animal either advanced toward or fled from the predatory threat irrespective of the robot-responsiveness (red circles, robot cells; white circles, non-robot cells).

Our neurophysiological LA-PL model is generalizable to other fearful settings. In Pavlovian fear conditioning, our model predicts a PL preceding LA activity (and relatively balanced PL-LA spike synchrony) during nonspecific contextual fear and a ramp-up LA activity (and biased LA→PL spike synchrony) to cue, explicitly predicting impending danger. A recent report (*21*) of BLA→PL directionality in correlated firings during conditioned freezing to a discrete (tone or light) CS is consistent with our proposition. Likewise, in signaled active avoidance, we predict a PL preceding LA activity (balanced PL-LA inputs) during the initial signal period before the animal makes avoidance response, and a ramp-up LA activity (biased LA→PL inputs) during the later signal period as the animal is about to make avoidance response. Our model further suggests the possibility that aberrant activity and spike synchrony in LA and PL underlie the complexity of fear-related psychopathologies (such as anxiety, phobic, panic, and posttraumatic stress disorders) that go beyond the strength of fear CRs (*34*, *35*). This translational prediction can be investigated using brain imaging techniques.

There is a need to confirm and extrapolate the neural responses revealed from fear conditioning studies to naturalistic danger settings where fear guides and shapes behaviors as animals make real-world choices. In addition, if predation has been a major driving force in the evolution of fear in animals and humans, then monitoring neural activities in behavioral paradigms that provide a greater match to the real-world threat situations will, at the very least, advance our understanding of the natural structure of the brain's fear system.

MATERIALS AND METHODS

Animals

Male Long-Evans rats (initially weighing 275 to 350 g) were individually housed in a climate-controlled vivarium (accredited by the Association for Assessment and Accreditation of Laboratory Animal Care) on a reverse 12-hour light/dark cycle (lights on at 7:00 p.m.). Animals were placed on a standard food deprivation schedule (with free access to water) to gradually reach and maintain 85% of their normal weight. All experiments were conducted during the dark phase of the cycle and in compliance with the University of Washington Institutional Animal Care and Use Committee guidelines.

Surgical procedures

Rats were anesthetized [ketamine (94 mg/kg, intraperitoneally) and xylazine (6 mg/kg, intraperitoneally)] and implanted with a microdrive array loaded with two bundles of three tetrodes in BLA (from bregma: 2.8 to 3.3 mm posterior, 5.2 mm lateral) and PL (from bregma: 3.2 mm anterior, 0.6 mm lateral). The microdrive array was embedded in dental cement with anchoring screws, one of which was used to fix the ground wire. All rats were given 6 to 7 days to recover from the surgery and habituated to handling before starting the experiment.

Foraging apparatus

A custom-built apparatus (Fig. 1B) consisted of a nest (approximate inner dimensions: 29 cm length × 57 cm width × 60 cm height; 16.2 lux luminance) and a V-shaped gate to an adjacent foraging area (202 cm length × 58 cm width × 61 cm height; 56.7 lux luminance; 60-dB white noise) tapered to a 21-cm-width floor by placing tilted inserts on either side. The animal's movement in both nesting and foraging areas was automatically tracked via light-emitting diodes mounted on the headstage and a video tracking system (Neuralynx).

Behavioral procedures

Hunger-motivated rats underwent habituation, baseline foraging, and robot testing days. Single-unit data were collected during the robot testing sessions.

Habituation

Rats were placed in the nesting area for 30 min/day for 2 days with 20 food pellets (500 mg, grain-based; F0171, Bio-Serv) to acclimate to the experimental room and to associate the nesting area with feeding.

Baseline

Two pellets were placed in the nest on the first baseline day (and none afterward). After pellets were consumed, the gateway to the foraging area opened, and animals were allowed to explore and search for a pellet placed 25 cm from the nest area (first trial). As soon as rats took the pellet and returned to the nest, the gateway closed. Once animals consumed the pellet, successive foraging trials ensued with a gradual increase of the pellet distance (that is, 50, 75, 100, and 125 cm). After a couple of pellet trials on day 1, rats proceeded directly to the pellet and brought it back to the nest; it rarely exceeded the pellet location. Animals underwent 5 to 10 days of baseline foraging.

Robot testing

Single units were recorded throughout the three sequential pre-robot, robot, and post-robot phases (Fig. 1, A and B). The pellet location was fixed at 125 cm during the recording days. When the gate opened, rats were allowed to procure the pellet, and they were always successful (pre-robot phase; 5 to 10 trials). After the last pre-robot trial, the robot was positioned at the end of the foraging area (robot phase). Each time animals approached the vicinity (~25 cm) of the pellet, the robot surged 23, 60, or 140 cm (pseudorandom order at a velocity of ~75 cm/s) toward the pellet, snapped its jaws one to three times, and returned to its original position. During the robot phase, rats very rarely acquired the pellet. If rats attempted to procure the pellet within 10 s following the preceding robot activation, then the trial was excluded from the analysis to ensure the characterization of unit responsiveness. Therefore, the number of the robot trials varied between animals (4 to 13 trials). Afterward, animals were allowed to procure the pellet without the robot (post-robot phase; 5 to 10 trials). During the post-robot phase (in the absence of the robot), animals repeatedly obtained the pellet. The robot was built, and its actions were programmed by using the LEGO Mindstorms EV3 set.

Single-unit recording and analyses

A custom-designed microdrive array loaded with two bundles of three tetrodes (diameter, 14 μm; Kanthal) was used to record extracellular single units. The cut electrode tips were gold-plated to reduce impedances from 100 to 300 kilohms measured at 1 kHz. After the postoperative recovery period, tetrodes were gradually advanced toward the target areas while the rat underwent habituation and baseline foraging. Unit signals were amplified (×10,000), filtered (600 to 6 kHz), and digitized (32 kHz) by using a Cheetah data acquisition system (Neuralynx). An automatic spike-sorting program (Neuralynx SpikeSort3D software) and additional manual cutting were used to isolate single units, as described previously (*36*).

Cells were classified as putative pyramidal neurons and interneurons using a hierarchical unsupervised cluster analysis (*37*) based on the average spike width and firing rate of each cell (fig. S7). Most of the units were putative pyramidal neurons (LA, n = 329, 95.1%; PL, n = 391, 90.1%). Because excluding interneurons did not change the results (fig. S8), both types of units were included in the final analyses [compare with the studies of Burgos-Robles *et al.* (*21*) and Quirk *et al.* (*27*)].

Peri-event time histograms were generated by using Neuroexploer (version 5.030; Nex Technologies) and further analyzed with custom MATLAB codes. Unless otherwise noted, unit and speed data were binned at 0.5 s and aligned to the time when the robot was activated or when the rat reached the pellet. "ATZ" was defined as the three 0.5-s bins before robot activation or to the time when the rat reached the pellet. All data were normalized to 3.5-s pre-ATZ time period (z score) and tested within five bins subsequent to the onset of ATZ. If the z score was higher than 3 ($z > 3$) in one or more bins during the robot phase and less than 3 ($z < 3$) during the pre-robot phase, then the units were classified as robot cells. If the opposite pattern was observed ($z > 3$ during the pre-robot phase; $z < 3$ during the robot phase), then the units were classified as "food cells." Among the robot cells, if a cell's maximal firing was shown before or after the robot was activated, the unit was classified as an "RA cell" or an "RT cell," respectively. Among the food cells, if a cell's maximal firing was shown before or after the food pellet was obtained, the unit was classified as an "FA cell" or an "FT cell," respectively. Because very low baseline firing rates can inflate z scores, if the pre-ATZ baseline firing rate was less than 0.1 Hz and/or the z score was higher than 30, then the z scores were expressed as the difference between the mean baseline firing rate and each bin value (and not divided by the SD) (*38*, *39*). FT cells were not further analyzed because the rats were unable to get the pellet during the robot phase. For the maximal response latency analysis, unit responses were binned at 0.1 s, and the peak unit response times during the testing windows were compared between the LA and PL cells.

Cross-correlation

CCs (10-ms bins) of the simultaneously recorded LA and PL cell pairs were generated (Neuroexplorer) for the pre-surge and surge epochs, with PL cells as references. Cells that sparsely fired during the pre- or post-surge epochs (less than 0.1 Hz in LA or PL) were excluded because they often produce false peaks in their CCs (*13*, *40*). The shift predictors generated by applying 100 random trial shuffles were subtracted from the raw CCs. Among the valid cell pairs, CCs showing significant peaks ($z > 3$) around the PL spikes (between −100 and 100 ms) during the pre-surge or surge epochs were further analyzed. Spike synchrony changes were determined by comparing 20 bins around the reference PL spikes (between −100 and 100 ms) across the (i) pre-surge (robot phase), (ii) post-surge (robot phase), and (iii) pre-pellet or post-pellet (pre-robot phase) epochs with RM ANOVAs followed by Bonferroni tests.

Histology

Electrolytic currents (10 μA, 20 s) were applied through the tetrode tips to verify the electrode placement following the completion of the experiment. The rats were overdosed with Beuthanasia and perfused intracardially with 0.9% saline followed by 10% buffered formalin. The brains were removed and stored in 10% formalin overnight and then kept in 30% sucrose solution until they sank. Transverse sections (50 μm) around the marking lesions were taken, mounted on gelatin-coated slides, and stained with cresyl violet and Prussian blue dyes.

Statistical analyses

Repeated-measures ANOVAs were performed to compare the dependent variables across pre-robot, robot, and post-robot phases, followed by multiple comparisons with a Bonferroni correction when necessary. Pearson's correlation coefficients were calculated to assess the relationship between time and peak firing or between the movement speed and firing rate during the pertinent time periods. Independent-samples t tests were performed to compare the group values. Chi-square tests were used to compare the proportions of the different properties of single cells or CCs. SPSS (version 19) and custom Matlab programs were used for the statistical analyses. Graphs were made using GraphPad Prism (version 7.00) and Neuroexploer (version 5.030).

SUPPLEMENTARY MATERIALS

Supplementary material for this article is available at http://advances.sciencemag.org/cgi/content/full/4/4/eaar7328/DC1

fig. S1. Histological reconstructions of recording sites in LA and PL.
fig. S2. LA- and PL-both cells.
fig. S3. Robot cells and response latency.
fig. S4. Food-responsive LA and PL units.
fig. S5. Relationships of movement speeds and firing rates.
fig. S6. Putative LA- and PL-leading CCs and their projections during risky foraging in rats.
fig. S7. Distribution of the cell types in LA and PL.
fig. S8. Robot-responsive neuronal activities from putative LA and PL pyramidal cells.

REFERENCES AND NOTES

1. R. C. Bolles, Species-specific defense reactions and avoidance learning. *Psychol. Rev.* **77**, 32–48 (1970).
2. B. A. Pellman, J. J. Kim, What can ethobehavioral studies tell us about the brain's fear system?. *Trends Neurosci.* **39**, 420–431 (2016).
3. M. S. Fanselow, L. S. Lester, A functional behavioristic approach to aversively motivated behavior: Predatory imminence as a determinant of the topography of defensive behavior, in *Evolution and Learning*, R. C. Bolles, M. D. Beecher, Eds. (Earlbaum, 1988), pp. 185–211.
4. J. E. LeDoux, Emotion circuits in the brain. *Annu. Rev. Neurosci.* **23**, 155–184 (2000).
5. S. Maren, Neurobiology of Pavlovian fear conditioning. *Annu. Rev. Neurosci.* **24**, 897–931 (2001).
6. D. Paré, G. J. Quirk, J. E. Ledoux, New vistas on amygdala networks in conditioned fear. *J. Neurophysiol.* **92**, 1–9 (2004).
7. J. B. Watson, R. Rayner, Conditioned emotional reaction. *J. Exp. Psychol.* **3**, 1–14 (1920).
8. J. J. Kim, M. W. Jung, Neural circuits and mechanisms involved in Pavlovian fear conditioning: A critical review. *Neurosci. Biobehav. Rev.* **30**, 188–202 (2006).
9. D. C. Blanchard, R. J. Blanchard, Innate and conditioned reactions to threat in rats with amygdaloid lesions. *J. Comp. Physiol. Psychol.* **81**, 281–290 (1972).
10. H. Klüver, P. C. Bucy, Preliminary analysis of functions of the temporal lobes in monkeys. *Arch. Neurol. Psychiatry* **42**, 979–1000 (1939).
11. P. MacLean, Psychosomatic disease and the "visceral brain": Recent developments bearing on the Papez theory of emotion. *Psychosom. Med.* **11**, 338–353 (1949).
12. P. Tovote, J. P. Fadok, A. Lüthi, Neuronal circuits for fear and anxiety. *Nat. Rev. Neurosci.* **16**, 317–331 (2015).
13. A. Burgos-Robles, I. Vidal-Gonzalez, G. J. Quirk, Sustained conditioned responses in prelimbic prefrontal neurons are correlated with fear expression and extinction failure. *J. Neurosci.* **29**, 8474–8482 (2009).
14. J. Lesting, T. Daldrup, V. Narayanan, C. Himpe, T. Seidenbecher, H.-C. Pape, Directional theta coherence in prefrontal cortical to amygdalo-hippocampal pathways signals fear extinction. *PLOS ONE* **8**, e77707 (2013).
15. E. Likhtik, J. M. Stujenske, M. A. Topiwala, A. Z. Harris, J. A. Gordon, Prefrontal entrainment of amygdala activity signals safety in learned fear and innate anxiety. *Nat. Neurosci.* **17**, 106–113 (2014).
16. J. LeDoux, The amygdala. *Curr. Biol.* **17**, R868–R874 (2007).
17. J. Muller, K. P. Corodimas, Z. Fridel, J. E. LeDoux, Functional inactivation of the lateral and basal nuclei of the amygdala by muscimol infusion prevents fear conditioning to an explicit conditioned stimulus and to contextual stimuli. *Behav. Neurosci.* **111**, 683–691 (1997).
18. W. B. Hoover, R. P. Vertes, Anatomical analysis of afferent projections to the medial prefrontal cortex in the rat. *Brain Struct. Funct.* **212**, 149–179 (2007).
19. A. J. McDonald, Organization of amygdaloid projections to the prefrontal cortex and associated striatum in the rat. *Neuroscience* **44**, 1–14 (1991).
20. K. A. Corcoran, G. J. Quirk, Activity in prelimbic cortex is necessary for the expression of learned, but not innate, fears. *J. Neurosci.* **27**, 840–844 (2007).
21. A. Burgos-Robles, E. Y. Kimchi, E. M. Izadmehr, M. J. Porzenheim, W. A. Ramos-Guasp, E. H. Nieh, A. C. Felix-Ortiz, P. Namburi, C. A. Leppla, K. N. Presbrey, K. K. Anandalingam, P. A. Pagan-Rivera, M. Anahtar, A. Beyeler, K. M. Tye, Amygdala inputs to prefrontal

cortex guide behavior amid conflicting cues of reward and punishment. *Nat. Neurosci.* **20**, 824–835 (2017).
22. J.-S. Choi, J. J. Kim, Amygdala regulates risk of predation in rats foraging in a dynamic fear environment. *Proc. Natl. Acad. Sci. U.S.A.* **107**, 21773–21777 (2010).
23. E. J. Kim, M. Park, M.-S. Kong, S. G. Park, J. Cho, J. J. Kim, Alterations of hippocampal place cells in foraging rats facing a "predatory" threat. *Curr. Biol.* **25**, 1362–1367 (2015).
24. S. K. Barot, A. Chung, J. J. Kim, I. L. Bernstein, Functional imaging of stimulus convergence in amygdalar neurons during Pavlovian fear conditioning. *PLOS ONE* **4**, e6156 (2009).
25. F. Gore, E. C. Schwartz, B. C. Brangers, S. Aladi, J. M. Stujenske, E. Likhtik, M. J. Russo, J. A. Gordon, C. D. Salzman, R. Axe, Neural representations of unconditioned stimuli in basolateral amygdala mediate innate and learned responses. *Cell* **162**, 134–145 (2015).
26. C.-h. Chang, J. D. Berke, S. Maren, Single-unit activity in the medial prefrontal cortex during immediate and delayed extinction of fear in rats. *PLOS ONE* **5**, e11971 (2010).
27. G. J. Quirk, C. Repa, J. E. LeDoux, Fear conditioning enhances short-latency auditory responses of lateral amygdala neurons: Parallel recordings in the freely behaving rat. *Neuron* **15**, 1029–1039 (1995).
28. J. C. Repa, J. Muller, J. Apergis, T. M. Desrochers, Y. Zhou, J. E. LeDoux, Two different lateral amygdala cell populations contribute to the initiation and storage of memory. *Nat. Neurosci.* **4**, 724–731 (2001).
29. E. J. Kim, O. Horovitz, B. A. Pellman, L. M. Tan, Q. Li, G. Richter-Levinand, J. J. Kim, Dorsal periaqueductal gray-amygdala pathway conveys both innate and learned fear responses in rats. *Proc. Natl. Acad. Sci. U.S.A.* **110**, 14795–14800 (2013).
30. A. Amir, S.-C. Lee, D. B. Headley, M. M. Herzallah, D. Pare, Amygdala signaling during foraging in a hazardous environment. *J. Neurosci.* **35**, 12994–13005 (2015).
31. J. Iwata, K. Chida, J. E. LeDoux, Cardiovascular responses elicited by stimulation of neurons in the central amygdaloid nucleus in awake but not anesthetized rats resemble conditioned emotional responses. *Brain Res.* **418**, 183–188 (1987).
32. J. P. Johansen, H. Hamanaka, M. H. Monfils, R. Behnia, K. Deisseroth, H. T. Blair, J. E. LeDoux, Optical activation of lateral amygdala pyramidal cells instructs associative fear learning. *Proc. Natl. Acad. Sci. U.S.A.* **107**, 12692–12697 (2010).
33. L. Lanteaume, S. Khalfa, J. Régis, P. Marquis, P. Chauvel, F. Bartolomei, Emotion induction after direct intracerebral stimulations of human amygdala. *Cereb. Cortex* **17**, 1307–1313 (2007).
34. S. Lissek, A. S. Powers, E. B. McClure, E. A. Phelps, G. Woldehawariat, C. Grillon, D. S. Pine, Classical fear conditioning in the anxiety disorders: A meta-analysis. *Behav. Res. Ther.* **43**, 1391–1424 (2005).
35. M. B. VanElzakker, M. K. Dahlgren, F. C. Davis, S. Dubois, L. M. Shin, From Pavlov to PTSD: The extinction of conditioned fear in rodents, humans, and anxiety disorders. *Neurobiol. Learn. Mem.* **113**, 3–18 (2014).
36. J. J. Kim, H. J. Lee, A. C. Welday, E. Song, J. Cho, P. E. Sharp, M. W. Jung, H. T. Blair, Stress-induced alterations in hippocampal plasticity, place cells, and spatial memory. *Proc. Natl. Acad. Sci. U.S.A.* **104**, 18297–18302 (2007).
37. J. J. Letzkus, S. B. E. Wolff, E. M. M. Meyer, P. Tovote, J. Courtin, C. Herry, A. Lüthi, A disinhibitory microcircuit for associative fear learning in the auditory cortex. *Nature* **480**, 331–335 (2011).
38. M. R. Gilmartin, M. D. McEchron, Single neurons in the medial prefrontal cortex of the rat exhibit tonic and phasic coding during trace fear conditioning. *Behav. Neurosci.* **119**, 1496–1510 (2005).
39. K. A. Goosens, J. A. Hobin, S. Maren, Auditory-evoked spike firing in the lateral amygdala and Pavlovian fear conditioning: Mnemonic code or fear bias?. *Neuron* **40**, 1013–1022 (2003).
40. X. Ye, D. Kapeller-Libermann, A. Travaglia, M. C. Inda, C. M. Alberini, Direct dorsal hippocampal-prelimbic cortex connections strengthen fear memories. *Nat. Neurosci.* **20**, 52–61 (2017).

Acknowledgments

Funding: This study was supported by the NIH grant MH099073 (to J.J.K.) and the Ministry of Science and Information & Communication Technologies through the National Research Foundation of Korea (NRF) grant: Brain Science Research Program (NRF-2015M3C7A1028392) (to J.C.). **Author contributions:** E.J.K., J.C., and J.J.K. designed the research. E.J.K. and M.-S.K. performed the research. E.J.K., M.-S.K., S.G.P., S.J.Y.M., J.C., and J.J.K. analyzed the data. E.J.K., S.J.Y.M., J.C., and J.J.K. wrote the paper. **Competing interests:** The authors declare that they have no competing interests. **Data and materials availability:** All data needed to evaluate the conclusions in the paper are present in the paper and/or the Supplementary Materials. Additional data related to this paper may be requested from the authors.

Submitted 12 December 2017
Accepted 2 March 2018
Published 18 April 2018
10.1126/sciadv.aar7328

Citation: E. J. Kim, M.-S. Kong, S. G. Park, S. J. Y. Mizumori, J. Cho, J. J. Kim, Dynamic coding of predatory information between the prelimbic cortex and lateral amygdala in foraging rats. *Sci. Adv.* **4**, eaar7328 (2018).